Accurate microthermometer based on off center polymer caps onto optical fiber tips

Oskar Arrizabalaga[1], Gaizka Durana[1], Joseba Zubia[1], Joel Villatoro[1,2*]

[1]Department of Communications Engineering, Escuela de Ingenieria de Bilbao, University of the Basque Country (UPV/EHU), Plaza Ingeniero Torres Quevedo 1, E-48013 Bilbao, Spain
[2]IKERBASQUE -Basque Foundation for Science, E-48011 Bilbao, Spain
[*]Corresponding author: agustinjoel.villatoro@ehu.eus

Abstract

We report on microscopic polymer spherical caps bonded onto the cleaved end of a single-mode fiber (SMF) for fast, accurate, and sensitive temperature sensing. The microcaps were fabricated by dispensing sub nano-liter amounts of UV-curable polymer onto the end face of a standard SMF that was cleaved at a small angle. A reflection from the SMF-polymer interface combined with a reflection from the polymer-external medium interface gives rise to a well-defined interference pattern. The high thermal expansion coefficient of the polymer used to build the micro-caps allowed us to achieve temperature sensitivity up to 270 pm/ºC, resolution of 0.04 ºC, and thermal response time of around 2.5 s. The simple fabrication process and the broad operating wavelength (from 800 to 1600 nm, approximately) of our devices along with the diversity of polymers currently available, make the concept and approach proposed here appealing for diverse sensing applications.

Keywords: Optical fiber sensors, Fabry-Perot interferometers, polymer cavity, temperature sensors, microsensors.

1. Introduction

As part of safety and quality control in industrial production, temperature is a crucial parameter that must be monitored or controlled. In environmental and bio-medical applications, temperature is also a parameter that is monitored constantly. As optical fiber temperature sensors (or thermometers) are capable of operating, hence to gather data, in environments where electromagnetic, radio frequency, or microwave radiation is present, they have gained considerable attention in the industrial and bio-medical sectors.

The fiber optic sensor community has exploited different methods and techniques to devise point optical fiber thermometers that include mode interferometers [1-4] and long period gratings (LPG) [5-8]. Such temperature sensors are robust and highly sensitive but their response time is slow, typically of several seconds. Moreover, in most cases, the sensitive segment of such thermometers is several millimeters, and even of centimeters, long. This makes them unsuitable for applications where space is small. To the authors' best knowledge, point thermometers based on mode interferometers or LPGs have not reached commercial level yet.

Other fiber optic temperature sensors reported so far are based on Fabry-Perot interferometry. The cavity, i.e., the sensitive element of the interferometers, can be made with a short segment of glass [9-11], polymer [12-15], or silicon [16,17]. These types of sensors are compact and highly sensitive. However, elaborated or multistep fabrication processes are required to achieve highly uniform cavities, hence high performance Fabry-Perot interferometers or thermometers.

To the authors' best knowledge, the most accurate fiber optic thermometers exploit the temperature dependence of fiber Bragg gratings (FBGs) [18-23], fluorescent materials [24-29], or GaAs semiconductor crystals [30,31]. The level of maturity of such techniques is high to a point that they have reached commercial level [32]. The main characteristics of thermometers based on FBGs include a sensitive segment of several millimeters in length (the length of the grating); thermal response time of several seconds, and temperature sensitivity of around 10 pm/ºC [18-23]. FBG thermometers tend to be expensive as their interrogation requires a pico-meter resolution detection system. On the other hand, thermometers based on fluorescent materials or semiconductor crystals are characterized by a fast response time, a sensitive material of few hundred micrometers in length or diameter attached to the end of a multimode optical fiber. The assembly of thermometers based on the aforementioned materials is complex. In addition, they can operate in short distances (a few tens of meters) as the fluorescent signal is low because they operate in non-telecommunications wavelengths.

As an alternative to the fiber optic thermometers discussed above, in this paper we propose an accurate interferometric thermometer that has the following remarkable features: *i*) microscopic dimensions, *ii*) simple fabrication and interrogation, and *iii*) operation over a wide wavelength range, from 800 to 1600 nm, approximately. Our device can sense temperature from -25 to 125 ºC with high sensitivity (up 270 pm/ºC) and fast response time (2.5 s). The sensitive section of our microthermometer is made of a UV curable polymer that is deposited onto the end face of a single mode fiber (SMF) that is cleaved at a small angle. As a result, an off center spherical microcap is formed. Light reflected from the SMF-polymer interface is

2

combined with that reflected from the polymer-external-medium interface. Due to the asymmetry of the two reflecting surfaces, the interference pattern exhibits a well-defined series of maxima and minima. We found that our sensors are as accurate as commercial electronic thermometers. Thus, we believe that the temperature sensors here proposed can be used in a variety of practical applications that require high sensitivity, fast thermal response, and miniature dimensions.

2. Sensor fabrication and operation principle

Our device consists of a microscopic polymer spherical cap formed on the end face of a standard single mode fiber (SMF) which is cleaved at a small angle. It is depicted in Fig. 1(a). The experimental set-up used to create such a microscopic spherical cap is shown schematically in Fig. 1(b). The fabrication steps are as follows. Firstly, two SMFs are cleaved with a conventional fiber optic cleaver. In our case, we used a <u>cleaver</u> from Fujikura, model CT-32. The typical cleave angle, i.e., the most probably angle, that is achieved with such a cleaver is ~0.5°. The cleaved optical fibers were cleaned with alcohol in an ultrasonic cleaner, and then they were clamped in separate 3-axis optical fiber alignment stages (ULTRAlign^{TM}, Newport). In our arrangement, the SMFs were placed in vertical position for the reasons explained below. One of the SMFs was the sensing fiber and the other one was used as a dispensing fiber. Our set up had also a CMOS USB camera to monitor the deposition of the polymer on the SMF face. To optimize the alignment between the SMFs, as well as to monitor the interference pattern of the samples, light from a super luminescent diode (SLD) was launched to the sensing SMF; the reflected light was sent to a mini-spectrometer by means of a suitable optical fiber coupler, see Fig. 1(b). The interference patterns were observed, stored, and analyzed, in a personal computer.

The dispensing SMF was dipped into a liquid polymer and then, it was gently withdrawn. The polymer we used is commercially known as NOA81 (from Norland Products Inc.). We used such polymer because it is cured in seconds and has excellent adhesion to glass. However, other polymers that can be bounded to glass can be used. After withdrawing the dispensing fiber from the liquid polymer, the fiber tip and the sides were coated with polymer, see the photograph shown in Fig. 1(c). The polymer-coated SMF was placed beneath, and in close proximity, to the sensing SMF. Immediately after that, the fibers were aligned with the 3- axis stages. The alignment between the SMFs was stopped when a well defined interference pattern was observed. Such an interference pattern was due to an air cavity formed between the facet of the sensing SMF and the liquid polymer covering the dispensing SMF. Afterwards, the
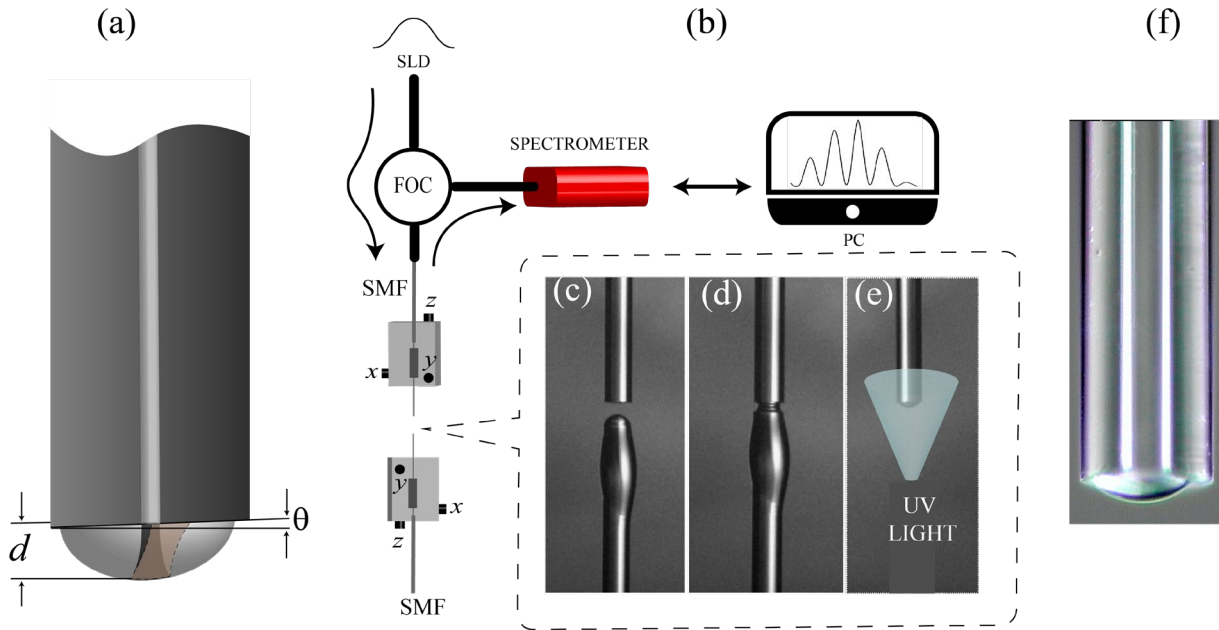
Figure 1. (a) Illustration of the temperature microsensor, d is the height of polymer microcap and θ the fiber cleave angle. (b) Schematic representation of the set-up used to monitor the fabrication process and to interrogate the devices. (c), (d) and (e) Sensor fabrication steps. SLD is superluminescent diode, SMF, single mode fiber, FOC, fiber optic coupler, and PC, personal computer. (f) Micrograph of an as-fabricated sample where d was 20 μm.

polymer-coated SMF was moved towards the sensing SMF until the polymer touched the end face of the sensing SMF, see Fig. 1(d). The dispensing SMF was then displaced far away from the sensing SMF; see Fig, 1(e).

It can be noted from the photograph that, due to surface tension, a microscopic polymer spherical cap is formed only onto the end face of the sensing SMF. The small angle of the SMF face makes the polymer microcap to be off center. In the final step of the fabrication process, the polymer was cured by illuminating it with UV light, with peak emission at 365 nm (CS2010, UV Curing LED System from Thorlabs), during 30 seconds. Under these conditions, the polymer spherical microcap becomes solid, and it is strongly bonded to the SMF. As recommended by the polymer manufacturer, for an optimum adhesion, the microcap was aged at 50 ºC during 12 hours. If other polymers are used, probably such an aging process is not necessary.

The interference patterns of our devices were analyzed after the fabrication process. The samples were also inspected under an optical microscope. After a single deposition process, d was found to be ~20 μm. This suggests that the volume of the spherical microcap, or the volume of polymer deposited on the SMF facet was on the order of ~ 0.15 nano-liters.

The operating principle of our sensor is explained as follows. Let us assume that a wave with amplitude E_0 propagates without attenuation in the core of the SMF, see Fig. 1(a). When such a wave reaches the SMF-polymer interface, it is partially reflected, the rest is transmitted to the polymer. The amplitude of the reflected wave (E_{r1}) can be expressed as:

$$E_{r1} = r_1 E_0, \tag{1}$$

where r_1 is the amplitude reflection coefficient which depends on the refractive indices of the polymer (n_p) and the fiber core (n_c), as $r_1 \approx (n_p-n_c)/(n_p+n_c)$. It is important to point out that the expression for r_1 is valid for quasi-perpendicular incidence and random polarized light. The wave that propagates in the polymer reaches the polymer-external-medium interface with an accumulated phase of $\phi = 2\pi n_p d/\lambda$, with d is the height of the polymer microcap and λ is the wavelength of the optical source. Such a wave suffers Fresnel reflection from the polymer-external-medium interface if the index of the polymer, n_p, and the refractive index of the external medium (n_e) are different.

The amplitude of the reflected wave (E_{r2}) can be expressed as $E_{r2} = E_0 r_2 (1-r_1) exp(-i\phi)$ where r_2 is the amplitude reflection coefficient which is expressed as $r_2 \approx (n_e-n_p)/(n_e+n_p)$. In our experiments, the external medium was air ($n_e = 1$). In our devices, not all the reflected wave from the polymer-external medium interface is coupled into the SMF core. Due to the small angle of the SMF face, the fiber facet and the curved surface of the polymer microcap are not parallel. That is the reason we do not treat our devices as a Fabry-Perot interferometer.

The reflected wave that is coupled back to the SMF core be expressed as:

$$E_c = \eta r_2 E_0 (1-r_1)^2 \exp(-i2\phi). \tag{2}$$

In Eq. (2), η is the coupling coefficient that can be calculated from Eqs. A7 and A8 given in Ref. [33]. According to the latter reference, η depends on the angle of the SMF face, d, n_p, λ, spot size of the output beam of the SMF, etc.

The amplitude of the total reflected field (E_T) is the sum of E_{r1} and E_c:

$$E_T = E_0 \left[r_1 + \eta r_2 (1-r_1)^2 \exp(-i2\phi) \right]. \tag{3}$$

Thus, the total reflected intensity that can be measured is $(E_T)^2$. By defining $I_r = (E_T/E_0)^2$ we get

$$I_r = r_1^2 + \eta^2 r_2^2 (1-r_1)^4 + 2\eta r_1 r_2 (1-r_1)^2 \cos(2\phi). \tag{4}$$

From Eq. (4), it can be deduced that I_r will be maximum when $\phi = 2m\pi$ and minimum when $\phi = (2m+1)\pi$, m being a positive integer. Thus, the peaks of the interference pattern (maximum values of I_r) are found at wavelengths that satisfy the condition:

$$\lambda_m = (2n_p d)/m. \tag{5}$$

Note also from Eq. (4) and (5) that η, that depends on the cleaved angle of the SMF, d, n_p, etc., will affect only on the contrast (or visibility) of the interference pattern but not the position of the maxima.

The temperature effect on our devices can be obtained by differentiating Eq. (5) with respect to temperature (T). We obtain:

$$\frac{\partial \lambda_m}{\partial T} = \left[\frac{1}{n_p} \frac{\partial n_p}{\partial T} + \frac{1}{d} \frac{\partial d}{\partial T} \right] \lambda_m. \tag{6}$$

The terms, $\partial n_p / \partial T$ and $\partial d / \partial T$, in Eq. (6) are, respectively, the thermo-optic coefficient (TOC) and the thermal expansion coefficient (TEC) of the material the microcap is made of. The refractive index of the polymer depends also on the wavelength of the optical source. According to the manufacturer, for the case of the NOA81 polymer, $n_p = A + B/\lambda^2 + C/\lambda^4$, with $A = 1.5375$, $B = 8290.45$, and $C = -2.11046 \times 10^8$; the TOC value is $-1.83 \times 10^{-4}/°C$ and the TEC value is $2.4 \times 10^{-4}/°C$.

From Eqs. (5) and (6), it can be concluded that the position of λ_m (a parameter that is easy to monitor) and the thermal sensitivity depend only on the TEC and TOC of the polymer used to fabricate the microcap. As the TEC value is higher that the TOC value of the NOA81 polymer, λ_m will shift to longer wavelengths <u>when</u> temperature increases. It should be point out that if other polymer is used to fabricate the sensor where the TOC be higher than the TEC, the shift of the interference pattern will be to shorter wavelengths when temperature increases.

Regardless the direction of the shift, temperature will be codified in wavelength, an absolute parameter, similar to FBG-based or semiconductor-based temperature sensors [18-23], [30,31].

3. Experimental results and discussion

To evaluate our devices as temperature sensors, they were first encapsulated with miniature stainless steel tubes (from Omega Solutions Inc.). Then, they were placed inside a temperature calibrator (LTR-25/140, from Kaye) that operates from -25 ºC to 140 ºC. However, according to the manufacturer, the NOA81 polymer, once cured and aged, can withstand temperatures from -150 °C to 125°C. Thus, the calibration was carried out from -25 to +125 ºC. As a reference, a precision and calibrated commercial RTD -resistance temperature detector- (Pt100 HH804U from Omega®) was placed inside the temperature calibrator, together with our devices. The interrogation of our devices was carried out with the components described in Fig. 1.

In Fig. 2(a), we show the observed spectra at different temperatures of a sample with a polymer cap where $d \sim 20$ μm. The red shift of the interference pattern is evident. The calibration curve is shown in Fig. 2(b). The theoretical fitting was carried out by considering a coupling factor $\eta = 0.18$. It can be seen that the device does not show any hysteresis. From Fig. 2 we calculated the relationship between λ_m and T as
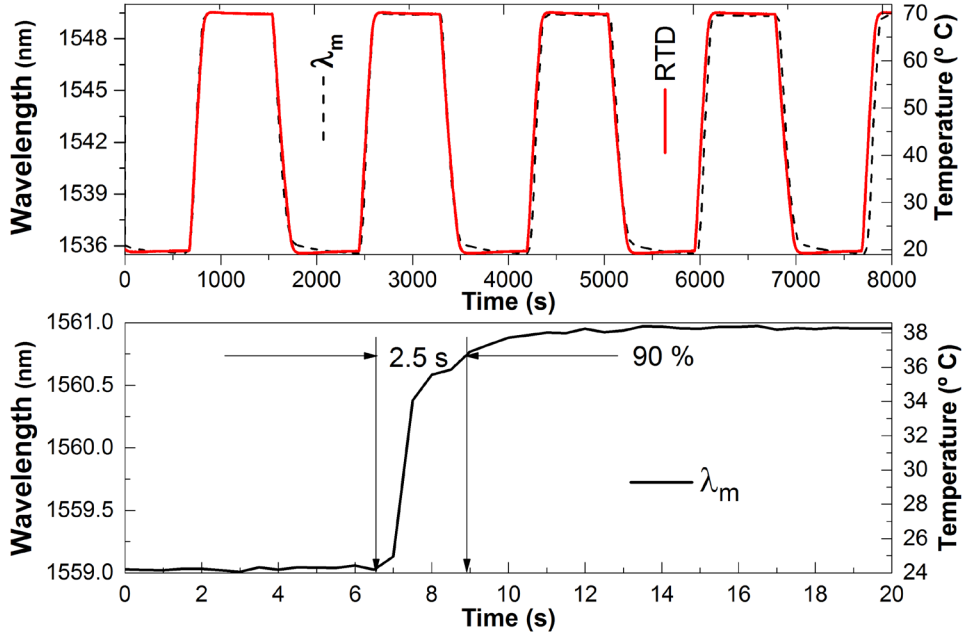
Figure 3. (a) Comparative between our sensor and the RTD of temperature pulses in the range of interest in medical applications. (b) Response time of the temperature sensor.

$$\lambda_m(nm) = 1535.99 + T \cdot (0.13 + 0.001 \cdot T - 7.96 \cdot 10^{-6} \cdot T^2) \qquad (7)$$
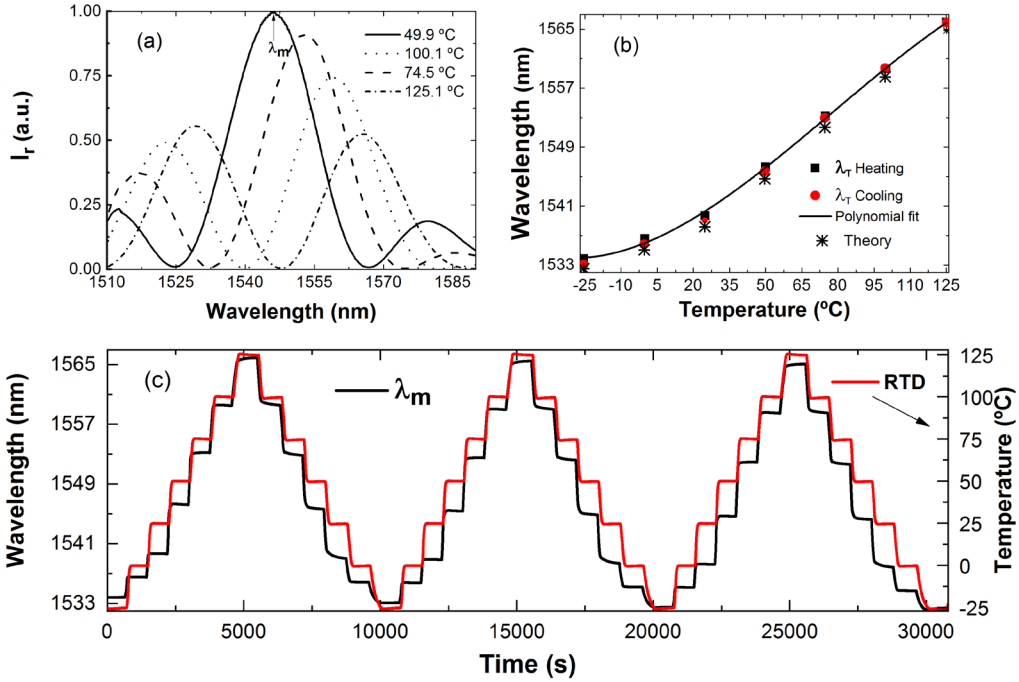

Figure 2. (a) Spectra of the temperature sensor at different temperatures. λ_m is the maximum of each spectrum. (b) Plot of λ_m versus temperature; the asterisks show the theoretical value of λ_m vs temperature and the squares and dots are experimental values. (c) Comparative of our temperature sensor with a commercial thermometer during several temperature cycles in steps of $\sim$ 25 degrees.

From the calibration curve, the temperature sensitivity in the <u>linear range, i.e.,</u> from 15 ℃ to 125 ℃, was found to be 270 pm/℃. Such sensitivity is an order of magnitude higher than that of FBG temperature sensors. With our interrogation system, the position of λ_m could be monitor with 10 pm precision. This means that our microthermometers can reach a resolution of 0.04 ℃.

An additional test to our samples consisted in exposing them repeatedly to several temperature cycles during more than 8 hours. The temperature was increased from – 25 ℃ to +125 ℃ in steps of 25 degrees. Then, the temperature was decreased <u>from +125 ℃ to -25 ℃ in steps of 25 ℃</u>. The results of our experiments are shown in Fig. 2(c). From the figure, it can be seen that our devices are as accurate as a commercial RTD.

Another test that we carried out consisted in the assessment of the response of our devices to temperature pulses, from 20 to 70℃. Such a temperature range was chosen because it is the range of interest in bio-medical applications. In Fig. 3(a) we show the results of our experiments. Again, we can see that our sensor provides accurate information as an RTD but the results suggest that our microthermometers respond faster than an RTD.

The response time of our devices was experimentally measured. For that, a microthermometer was encapsulated with a short segment of silica capillary of 150 µm and
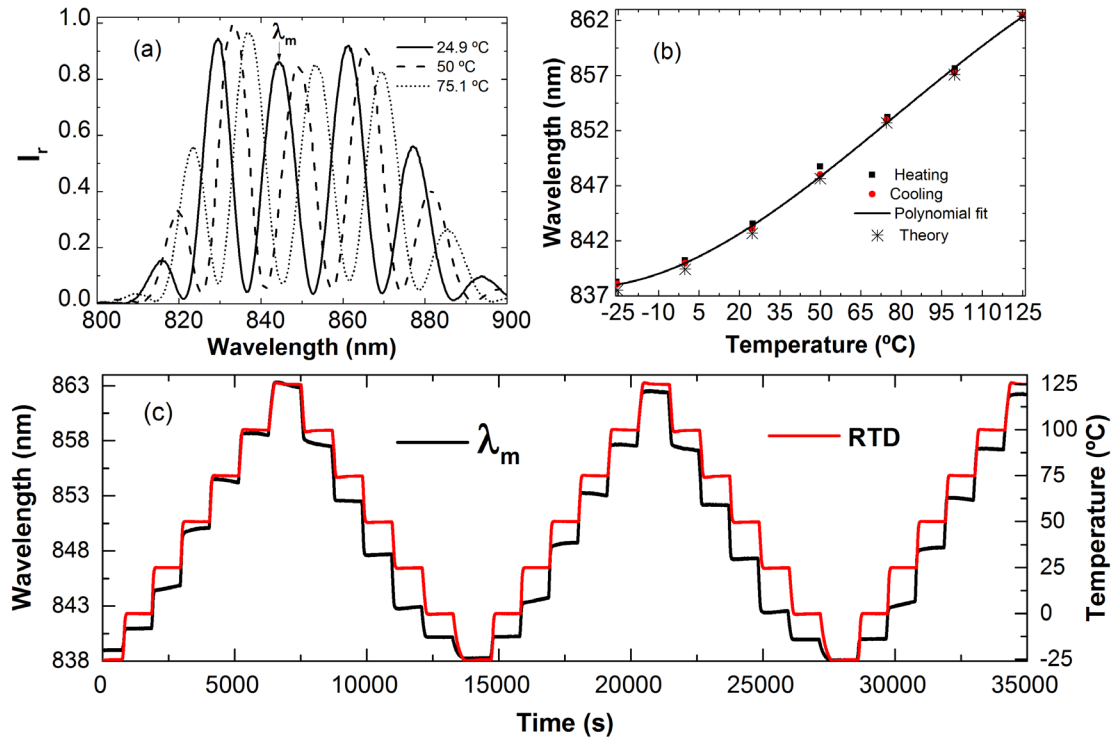
Figure 4. (a) Spectra at around 850 nm at different temperatures of a sample where the polymer microcap had a $d = 20$ μm. (b) Experimental and theoretical values (asteriks) of λ_m as a function of temperature. (c) Comparative of our temperature sensor with a commercial thermometer during several temperature cycles in steps of 25 degrees.

300 μm of inner and outer diameter, respectively. Our device was attached to an RTD, and then, they were immersed in hot water. The temperature of the hot water was monitored with the RTD. The temperature of the external environment was monitored with another RTD. Figure 3(b) shows the wavelength shift of our device under study as a function of time when the temperature increased from 24 to 37.9 ºC. From the figure, we calculated the thermal response time of our device. It was found to be 2.5 s. Such a response time is faster than that of other fiber optic temperature sensors, as for example, FBG-based thermometers.

We also fabricated and characterized some samples that operated at shorter wavelengths. To do so, we used an SMF at 850 nm (HP780, from Thorlabs). The deposition of the microcaps was carried out with the same steps described above. The height of the microcap was again ~20 μm. At shorter wavelengths, the refractive index of the polymer is higher. The combination of shorter wavelengths and higher index makes the period of the interference pattern larger at 850 nm. Figure 4(a) shows the output spectra of the quoted device at different temperatures. Again, a shift to longer wavelengths as the temperature increased was found. The calibration curve is shown in Fig. 4(b). Note the linear dependence of λ_m on temperature in the range from 15 to 125 ºC. In that range, the temperature sensitivity was found to be 210 pm/ºC. This suggests that there is no loss of temperature sensitivity at shorter wavelengths.

We also exposed the samples repeatedly to several temperature cycles during 10 hours approximately. The temperature was increased from -25 ºC to +125 ºC; and then it was decreased to -25 ºC. The steps were also 25 ºC. The results of our experiments are shown in Fig. 4(c). It can be noted from such a figure that our devices provide information of temperature as a well-calibrated RTD. An advantage of fiber optic thermometers that operate at 850 nm is the fact that light sources and spectrometers are less expensive. Hence, cost effective microthermometers can be developed.

4. Conclusions

We have reported on a micrometer-size fiber optic temperature interferometric sensors that is fast and accurate. The fabrication of our devices is simple and reproducible. An important advantage of our devices is that they operate at the well-established telecommunications wavelength bands. In our devices, the temperature sensitive region is a microscopic polymer spherical cap bonded onto the facet of a single mode optical fiber, which is cleaved at a small angle. Our devices have high temperature sensitivity and resolution and respond fast to temperature changes.

The performance of the sensors here proposed can be further improved. The science and technology of polymers is mature. Currently, polymers with tailored optical and physical properties can be synthesized. This may allow to tailor the thermal response time, temperature sensitivity, or operating temperature range of our devices.

We believe that the devices here proposed can be useful in several applications that demand miniature thermometers. For example, they can useful to explore temperature inside micro-fluid channels or other small spaces or to monitor temperature of tiny objects. Their fast thermal response time makes them attractive to monitor temperature in environmental or biomedical applications. Due to their passive nature, the microthermometers reported here can be attractive in industrial applications.

References

[1] W. Eickhoff, Temperature sensing by mode-mode interference in birefringent optical fibers, Opt. Lett. 6 (1981) 204-206. doi:10.1364/OL.6.000204.

[2] E. Li, X. Wang, C. Zhang, Fiber-optic temperature sensor based on interference of selective higher-order modes, Appl. Phys. Lett. 89 (2006) art. ID 091119. doi:10.1063/1.2344835.

[3] J.E. Antonio-Lopez, Z.S. Eznaveh, P. LiKamWa, A. Schülzgen, R. Amezcua-Correa, Multicore fiber sensor for high-temperature applications up to 1000°C, Opt. Lett. 39 (2014) 4309–4312. doi:10.1364/OL.39.004309.

[4] I. Hernandez-Romano, D. Monzon-Hernandez, C. Moreno-Hernandez, D. Moreno-Hernandez, J. Villatoro, Highly sensitive temperature sensor based on a polymer-coated microfiber interferometer, IEEE Photonics Technol. Lett. 27 (2015) 2591–2594. doi:10.1109/LPT.2015.2478790.

[5] V. Bhatia, A.M. Vengsarkar, Optical fiber long-period grating sensors, Opt. Lett. 21 (1996) 692–694. doi:10.1364/OL.21.000692.

[6] S. Khaliq, S.W. James, R.P. Tatam, Enhanced sensitivity fibre optic long period grating temperature sensor, Meas. Sci. Technol. 13 (2002) 792–795. doi:10.1088/0957-0233/13/5/318.

[7] S.K. Abi Kaed Bey, T. Sun, K.T. V Grattan, Optimization of a long-period grating-based Mach-Zehnder interferometer for temperature measurement, Opt. Commun. 272 (2007) 15–21. doi:10.1016/j.optcom.2006.11.016.

[8] C. Du, Q. Wang, Y. Zhao, J. Li, Highly sensitive temperature sensor based on an isopropanol-filled photonic crystal fiber long period grating, Opt. Fiber Technol. 34 (2017) 12–15. doi:10.1016/j.yofte.2016.11.013.

[9] C.E. Lee, H.F. Taylor, Fiber-optic Fabry-Perot temperature sensor using a low-coherence light source, J. Light. Technol. 9 (1991) 129–134. doi:10.1109/50.64932.

[10] H.Y. Choi, K.S. Park, S.J. Park, U.C. Paek, B.H. Lee, E.S. Choi, Miniature fiber-optic high temperature sensor based on a hybrid structured Fabry-Perot interferometer, Opt. Lett. 33 (2008) 2455–2457. doi:10.1364/OL.33.002455.

[11] S. Pevec and D. Donlagic, High resolution, all-fiber, micro-machined sensor for simultaneous measurement of refractive index and temperature, Opt. Express 22 (2014) 16241-16253. doi.org/10.1364/OE.22.016241.

[12] X.L. Tan, Y.F. Geng, X.J. Li, Y.L. Deng, Z. Yin, R. Gao, UV-curable polymer microhemisphere-based fiber-optic Fabry-Perot interferometer for simultaneous measurement of refractive index and temperature, IEEE Photonics J. 6 (2014) art. ID 7800208. doi:10.1109/JPHOT.2014.2332460.

[13] B. Sun, Y. Wang, J. Qu, C. Liao, G. Yin, J. He, J. Zhou, J. Tang, S. Liu, Z. Li, Y. Liu, Simultaneous measurement of pressure and temperature by employing Fabry-Perot interferometer based on pendant polymer droplet, Opt. Express, 23 (2015), 1906–1911.

[14] M. Li, Y. Liu, R. Gao, Y. Li, X. Zhao, S. Qu, Ultracompact fiber sensor tip based on liquid polymer-filled Fabry-Perot cavity with high temperature sensitivity, Sensors Actuators, B Chem. 233 (2016) 496–501. doi:10.1016/j.snb.2016.04.121.

[15] I. Hernández-Romano, M.A. Cruz-Garcia, C. Moreno-Hernández, D. Monzón-Hernández, E.O. López-Figueroa, O.E. Paredes-Gallardo, M. Torres-Cisneros, J. Villatoro, Optical fiber temperature sensor based on a microcavity with polymer overlay, Opt. Express. 24 (2016) 5654-5661. doi:10.1364/OE.24.005654.

[16] G. Liu, M. Han, W. Hou, High-resolution and fast-response fiber-optic temperature sensor using silicon Fabry-Pérot cavity, Opt. Express 23 (2015) 7237-7247. doi:10.1364/OE.23.007237.

[17] G. Liu, Q. Sheng, W. Hou, and M. Han, High-resolution, large dynamic range fiber-optic thermometer with cascaded Fabry–Perot cavities, Opt. Lett. 41 (2016) 5134-5137.

[18] A.D. Kersey, T.A. Berkoff, Fiber-optic Bragg-grating differential-temperature sensor, IEEE Photonics Technol. Lett. 4 (1992) 1183–1185. doi:10.1109/68.163773.

[19] Y.J. Rao, D.J. Webb, D.A. Jackson, L. Zhang, I. Bennion, In-fiber Bragg-grating temperature sensor system for medical applications, J. Light. Technol. 15 (1997) 779–784. doi:10.1109/50.580812.

[20] D. Grobnic, S.J. Mihailov, C.W. Smelser, H. Ding, Sapphire fiber Bragg grating sensor made using femtosecond laser radiation for ultrahigh temperature applications, IEEE Photon. Technol. Lett. 16 (2004) 2505–2507. doi:10.1109/LPT.2004.834920.

[21] B. Zhang, M. Kahrizi, High-temperature resistance Fiber Bragg grating temperature sensor fabrication, IEEE Sens. J. 7 (2007) 586–591. doi:10.1109/JSEN.2007.891941.

[22] Y. Zhan, S. Xue, Q. Yang, S. Xiang, H. He, R. Zhu, A novel fiber Bragg grating high-temperature sensor, Optik 119 (2008) 535–539. doi:10.1016/j.ijleo.2007.02.010.

[23] D. Barrera, V. Finazzi, J. Villatoro, S. Sales, V. Pruneri, Packaged optical sensors based on regenerated fiber Bragg gratings for high temperature applications, IEEE Sens. J. 12 (2012) 107–112. doi:10.1109/JSEN.2011.2122254.

[24] H. Berthou, C.K. Jörgensen, Optical-fiber temperature sensor based on upconversion-excited fluorescence, Opt. Lett. 15 (1990) 1100–1102. doi:10.1364/OL.15.001100.

[25] S.A. Wade, S.F. Collins, G.W. Baxter, Fluorescence intensity ratio technique for optical fiber point temperature sensing, J. Appl. Phys. 94 (2003) 4743–4756. doi:10.1063/1.1606526.

[26] S.A. Wade, S.F. Collins, G.W. Baxter, Fluorescence intensity ratio technique for optical fiber point temperature sensing, J. Appl. Phys. 94 (2003) 4743–4756. doi:10.1063/1.1606526.

[27] S. Baek, Y. Jeong, J. Nilsson, J.K. Sahu, B. Lee, Temperature-dependent fluorescence characteristics of an ytterbium-sensitized erbium-doped silica fiber for sensor applications, Opt. Fiber Technol. 12 (2006) 10–19. doi:10.1016/j.yofte.2005.04.002.

[28] S. Musolino, E.P. Schartner, G. Tsiminis, A. Salem, T.M. Monro, M.R. Hutchinson, Portable optical fiber probe for in vivo brain temperature measurements, Biomed. Opt. Express. 7 (2016) 3069-3077. doi:10.1364/BOE.7.003069.

[29] Y. Zhao, M.Q. Chen, R.Q. Lv, P. Wang, X. Feng, Small and practical optical fiber fluorescence temperature sensor, IEEE Trans. Instrum. Meas. 65 (2016) 2406–2411. doi:10.1109/TIM.2016.2575241.

[30] M. M. Salour, G. Schoner, M. Kull, J. H. Bechtel, Semiconductor-platelet fibre-optic temperature sensor, Electron. Lett. 21 (1985) 135-136.

[31] K. Kyuma, S. Tai, T. Sawada, M. Nunoshita, Fiber-optic instrument for temperature measurement, IEEE Trans. Microw. Theory Tech. 30 (1982) 522–525. doi:10.1109/TMTT.1982.1131092.

[32] É. Pinet, S. Ellyson, F. Borne, Temperature fiber-optic point sensors: Commercial technologies and industrial applications, Inf. MIDEM. 40 (2010) 273–284.

[33] Y. St-Amant, D. Gariépy, D. Rancourt, Intrinsic properties of the optical coupling between axisymmetric Gaussian beams, Appl. Opt. 43 (2004) 5691–704. doi:10.1364/AO.43.005691.